

Measurements of the spin relaxation rate at low magnetic fields in a quantum dot

S. Amasha,^{1,*} K. MacLean,¹ Iuliana Radu,¹ D. M. Zumbühl,^{1,2} M. A. Kastner,¹ M. P. Hanson,³ and A. C. Gossard³

¹*Department of Physics, Massachusetts Institute of Technology, Cambridge, Massachusetts 02139*

²*Department of Physics and Astronomy, University of Basel,*

Klingelbergstrasse 82, CH-4056 Basel, Switzerland

³*Materials Department, University of California, Santa Barbara 93106-5050*

We measure the relaxation rate $W \equiv T_1^{-1}$ of a single electron spin in a quantum dot at magnetic fields from 7 T down to 1.75 T, much lower than previously measured. At 1.75 T we find that T_1 is 170 ms. We find good agreement between our measurements and theoretical predictions of the relaxation rate caused by the spin-orbit interaction, demonstrating that spin-orbit coupling can account for spin relaxation in quantum dots.

PACS numbers: 73.63.Kv, 03.67.Lx, 76.30.-v

To implement proposals [1] for quantum computation based on manipulating electron spins [2] in quantum dots [3], the spin of the electron must remain coherent for a sufficiently long period of time. One decoherence mechanism that can affect this time is spin-orbit coupling [4]. In a magnetic field B the spin states of a single electron in a dot are split by the Zeeman energy $\Delta = |g|\mu_B B$. The energy relaxation time T_1 is the average time necessary for an electron in the excited spin state to relax to the ground spin state. In single quantum dots, it has been predicted [4, 5, 6] that spin relaxation is caused by the spin-orbit interaction and that T_1 increases with decreasing magnetic field. Pulsed gate transport measurements [7, 8] have put lower bounds on T_1 , while Elzerman *et al.* [9] have utilized an energy-selective spin readout technique to measure T_1 for one electron in a single dot at large magnetic fields and found $T_1 = 0.85$ ms at $B = 8$ T. Hanson *et al.* [10] have measured the singlet-triplet relaxation time at smaller fields for two electrons.

In this Letter, we present measurements of the relaxation rate $W \equiv T_1^{-1}$ of one electron in a single dot at magnetic fields from 7 T down to 1.75 T, much lower than previously measured. These measurements are possible because of the good stability of the heterostructure we used combined with an active feedback system that compensates for residual drift and switches of the dot energy levels, allowing us to measure down to fields where Δ is comparable to our electron temperature. We find relaxation times as long as 170 ms at 1.75 T. We compare our measurements of W vs B to theoretical predictions by Golovach *et al.* [4] of the relaxation rate caused by spin-orbit coupling and find excellent agreement between theory and experiment. This demonstrates that spin-orbit coupling can account for the relaxation of the spin of a single electron in a quantum dot.

The dot used in this work is fabricated from an AlGaAs/GaAs heterostructure. The two-dimensional electron gas (2DEG) formed at the AlGaAs/GaAs interface 110 nm below the surface has an electron density of $2.2 \times 10^{11} \text{ cm}^{-2}$ and a mobility of $6.4 \times 10^5 \text{ cm}^2/\text{Vs}$ [11]. The gate geometry is shown in Fig. 1(a) and is based on

that of Ciorga *et al.* [12]. We choose gate voltages so that we form a single dot containing one electron. For this work we have tuned the barrier formed by the gates OG and SG1 to have a tunnel rate much lower than the rate through the barrier defined by OG and SG2. We measure the dot in a dilution refrigerator with an electron temperature of about 120 mK. To minimize orbital effects we align the 2DEG parallel to the magnetic field to within a few degrees.

We use the quantum point contact (QPC) formed by SG2 and QG2 as a sensitive electrometer or charge sensor [13] for the dot. The detection circuit is illustrated in Fig. 1(a) and more details are in Refs. [14, 15, 16]. If an electron tunnels onto or off the dot, it changes the electrochemical potential of the electrons in the QPC, which in turn causes a change in resistance δR . We observe δR by sourcing a 1–2 nA current across the QPC and measuring the change in voltage δV_{QPC} . By making the tunneling rate through the OG-SG2 barrier less than the bandwidth of our circuit, we observe the electron tunneling in real time [9, 17, 18]. Our typical signal size of $10 \mu\text{V}$ is approximately 5% of the total voltage across the QPC; this good sensitivity may come from making the gate SG2 between the dot and the QPC narrow, which increases the coupling between the dot and the QPC [19]. The small QPC current does not heat the electrons, which is important because it is our electron temperature which sets the lower limit on the fields we can measure.

To measure W at a given magnetic field, we apply a three step pulse sequence [9] V_p on top of the dc voltage on gate LP2: $V_{\text{LP2}} = V_{\text{dc}} + V_p$. This sequence is illustrated in Fig. 1(e), where we have converted the gate voltage pulse V_p into the equivalent electrochemical potential energy change of the dot: $E_p = -e\alpha_{\text{LP2}}V_p$, where $\alpha_{\text{LP2}} \approx 0.065$ is the capacitance ratio for gate LP2 extracted from transport measurements [15]. The first step is to apply a negative V_p to bring both spin states above the Fermi energy of the lead, as shown in Fig. 1(b). We hold the dot in this configuration for a fixed time t_i , during which time the electron can tunnel off the dot. After

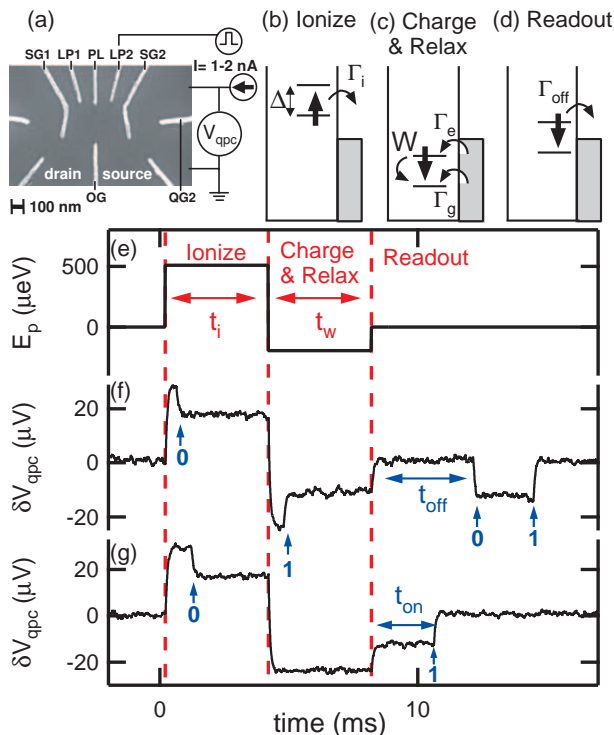


FIG. 1: (a) Electron micrograph of the gate geometry. Negative voltages are applied to the labeled gates to form the quantum dot and the QPC charge sensor; unlabeled gates are grounded. Pulses are applied to gate LP2. The drain and source electrodes are labeled and are grounded. (b)-(d) diagrams showing the configuration of energy levels for the three steps in the pulse sequence shown in (e). (f) and (g) are examples of data taken at $B = 2.5$ T and $t_w = 4$ ms. The direct capacitive coupling between LP2 and the QPC causes the QPC to respond to the pulse sequence; electron tunneling events are evident on top of this response. The 0's denote when an electron tunnels off the dot, while 1's denote when an electron tunnels on.

time t_i the dot is in one of three possible states: there is a probability P_i that the dot is ionized given by the ionization efficiency $\epsilon_i = 1 - e^{-\Gamma_i t_i}$, where Γ_i is the tunnel-off rate. In this work, $\epsilon_i \approx 0.95$. The probability of being in the ground state is $P_g \approx 1 - \epsilon_i$. Finally, the probability of being in the excited state is thermally suppressed and is $P_e = e^{-\Delta/k_B T} P_g$, which is negligible.

After ionizing the dot, we apply a positive V_p and bring both states below the Fermi energy of the lead as shown in Fig. 1(c). We hold the dot in this configuration for a time t_w , which we vary. During this time, electrons tunnel into either the ground or excited states of the dot with rates Γ_g and Γ_e , respectively. We expect that $\Gamma_e/\Gamma_t = 0.5$ where $\Gamma_t = \Gamma_e + \Gamma_g$, but we do not assume this a-priori, since we extract Γ_e/Γ_t from our measurements. During t_w , the electrons can relax from the excited to the ground state with a rate W . The

rate equations describing the model are $\dot{P}_i = -\Gamma_t P_i$ and $\dot{P}_e = \Gamma_e P_i - W P_e$. Solving these equations, we find that the probabilities of being in the three states after time t_w are given by

$$P_i(t_w) = \epsilon_i e^{-\Gamma_t t_w} \quad (1)$$

$$P_e(t_w) = \epsilon_i \frac{\Gamma_e}{\Gamma_t} \frac{\Gamma_t}{\Gamma_t - W} (e^{-W t_w} - e^{-\Gamma_t t_w}) \quad (2)$$

and $P_g = 1 - P_e - P_i$. It is important to note that in Eq. 2 the t_w dependence of P_e depends only on W and Γ_t . In particular, Eq. 2 has a maximum at $t_w = \ln(\Gamma_t/W)/(\Gamma_t - W)$. We can measure Γ_t from the t_w dependence of P_i and then use the t_w dependence of P_e to determine W .

The third step in the pulse sequence is the real-time readout, shown in Fig. 1(d). We follow Elzerman *et al.* [9] and position the levels so that the excited state is above the Fermi energy of the lead and the ground state is below the Fermi energy. In this configuration, an electron in the excited spin state can quickly tunnel off the dot with rate Γ_{off} , while the tunneling rate of an electron in the ground state is exponentially suppressed.

Figure 1(f-g) show examples of two types of data. In Fig. 1(f) we see that an electron tunnels off during the ionization pulse and back on during the charging pulse. When we enter the readout stage, an electron tunnels off the dot, presumably from the excited state, at a time t_{off} after the end of the charging pulse. Shortly after this, an electron tunnels back onto the empty dot. We call this behavior a ‘tunnel-off’ event. In contrast, in Fig. 1(g) we see an electron tunnel off during the ionization pulse, but no electron tunnels on during the charging pulse. Thus the dot is empty entering the readout stage and the first event in this stage is an electron tunneling onto the empty dot. We call this an ‘ionization event’, and measure the time t_{on} between the end of the charging pulse and the time when an electron tunnels onto the dot. The times t_{off} and t_{on} are measured using a triggering and acquisition system described in Ref. [15].

For a given t_w and B we repeat the pulse sequence N_{pulse} times, where N_{pulse} is typically between 1×10^4 and 1.5×10^5 . We histogram the measurements of t_{off} from tunnel-off events; the results are shown in Fig. 2(a) and (b) for two different sets of t_w and B . The data are fit well by an exponential on top of a constant offset. The exponential portion of the data is caused by fast tunneling out of the excited spin state (Fig. 2(c)), while the offset is caused by slow tunneling out of the ground spin state (Fig. 2(d)). Although the energy of the ground spin state is below the Fermi energy of the lead, there is still a slow rate for tunneling out of the ground state given by $\Gamma_b = \Gamma_{off}(1 - f(E_{dot}))/ (1 - f(E_{dot} + \Delta))$, where f is the Fermi function and $E_{dot} < 0$ is the depth of the

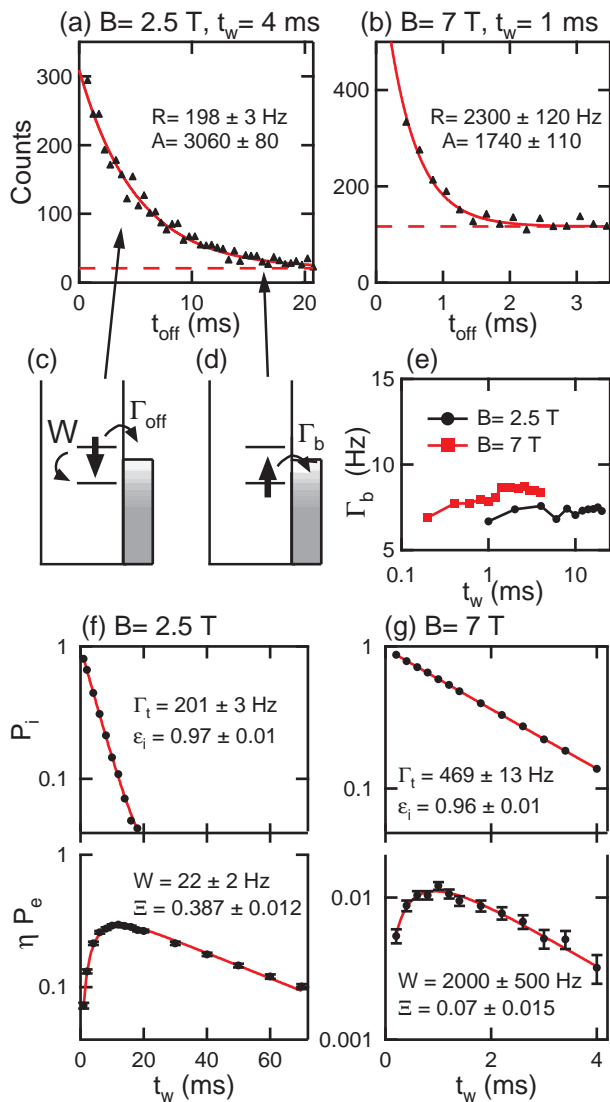


FIG. 2: (a)-(b) histograms of t_{off} for tunnel-off events for two different sets of B and t_w . The exponential is caused by fast tunneling of electrons out of the excited state illustrated in (c) while the offset is caused by slow tunneling out of the ground state as depicted in (d). The rate R is obtained by averaging over the exponentials for several values of t_w at each field. This averaging is possible because the readout configuration is the same for all t_w at a given field, so R is independent of t_w . (e) shows the rates Γ_b extracted from the offsets measured from data like those in (a) and (b). Γ_b is approximately constant for different t_w and between data sets because of the active feedback control discussed in the text. (f)-(g) show measured values of P_i and ηP_e at different B . The solid lines are fits to Eqs. 1 and 2 as discussed in the text.

ground state below the Fermi energy of the lead. Our electron temperature allows us to maintain E_{dot} so that $\Gamma_b \approx 8 \text{ Hz} \ll \Gamma_{off}$. The slow tunneling out of the ground state gives an exponential distribution; however, $1/\Gamma_b \approx 100 \text{ ms}$ is so long it appears as a constant offset.

The ground state tunneling rate Γ_b is useful for maintaining the stability of the levels in the quantum dot. As noted in previous work [10] the energy levels in lithographically defined quantum dots shift over time because of background charge fluctuations in the heterostructure [20]. In general, we observe two types of shifts: a slow drift of the levels over time and sudden, large shifts in the position of the energy levels. Our readout method is sensitive to these shifts because it requires that the ground spin state remain below the Fermi energy of the lead while the excited state remains above it. This is a difficult condition to maintain, especially at low B where Δ is small. Our heterostructure is relatively stable in this regard. In addition, we use active feedback to control the levels in the dot and compensate for these shifts. As noted above, the ground state tunneling rate Γ_b is a function of E_{dot} . We monitor Γ_b approximately every 15 s and then adjust a gate voltage to maintain E_{dot} such that $5 \lesssim \Gamma_b \lesssim 15 \text{ Hz}$. We extract Γ_b from the offset in the histograms in Fig. 2(a) and (b). These data are shown in Fig. 2(e). The rate is fairly constant over the range of t_w and between data sets, demonstrating the efficacy of our feedback control.

To measure P_e for a given t_w and B , we need to count the number of times N_e that the electron is in the excited state after the charging pulse. For $W \ll \Gamma_{off}$ the exponential decay should have rate $R = \Gamma_{off}$ and the area A under the exponential and above the offset gives N_e . If $W \approx \Gamma_{off}$, the interpretation is more complicated because an electron in the excited state might relax before it has a chance to tunnel off the dot [10]. In this case, the rate of the exponential is the rate at which electrons leave the excited state, namely $R = \Gamma_{off} + W$. Moreover, we only observe the fraction η of the electrons in the excited state that tunnel off before they relax given by $\eta = \Gamma_{off}/(\Gamma_{off} + W)$. Thus the area under the exponential and above the offset gives ηN_e and $\eta P_e = \eta N_e / N_{pulses}$. Measurements of ηP_e as a function of t_w at two different magnetic fields are shown in the lower panels of Fig. 2(f) and (g). It is important to note that the information about the relaxation rate W comes from the t_w dependence of P_e , hence the multiplicative factor η does not affect our ability to extract W .

We can also measure P_i as a function of t_w . We count the number of ionization events N_i like those in Fig. 1(g) by histogramming the values of t_{on} . The distribution is an exponential with no offset and the area underneath the exponential gives N_i ; dividing by N_{pulses} gives P_i . The upper panels of Fig. 2(f) and (g) show examples of P_i as a function of t_w at two different magnetic fields. We fit $P_i(t_w)$ to Eq. 1 (solid line) to obtain Γ_t and ϵ_i . While Γ_t may have some dependence on B , it has a much stronger dependence on the tunnel rate set by the gate voltages which may be different for measurements at different B . Using the value of Γ_t , we fit $\eta P_e(t_w)$ to Eq. 2 to find W and the prefactor $\Xi = \eta \epsilon_i \Gamma_e / \Gamma_t$. These fits, shown as the

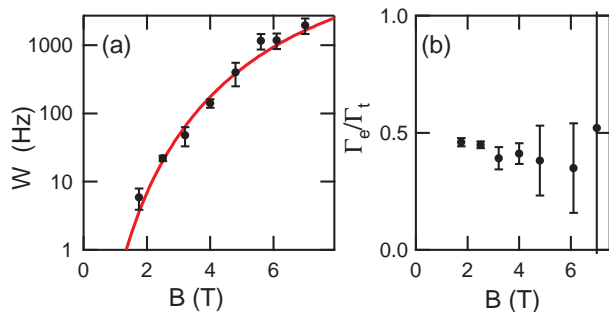


FIG. 3: (a) relaxation rate W as a function of magnetic field. The solid line is a theoretical prediction from the work of Golovach *et al.* [4] and is discussed in the text. (b) Γ_e/Γ_t as a function of magnetic field. From these data we see that Γ_e/Γ_t is independent of field and is close to 0.5. The data point at $B = 5.6$ is $\Gamma_e/\Gamma_t = 2.2 \pm 5.8$ and is not shown. The large errors result from a large error in η at this field.

solid lines in the lower panels in Fig. 2(f) and (g), give excellent agreement with our data.

From the upper and lower panels of Fig. 2(f) and (g), one can explicitly see the relationship between $P_i(t_w)$ and $P_e(t_w)$ in two different regimes. When $\Gamma_t > W$ (Fig. 2(f)), P_e increases on the time scale of Γ_t^{-1} and decays on the time scale of W^{-1} . When $W > \Gamma_t$ (Fig. 2(g)), P_e increases on the time scale of W^{-1} and decays on the scale of Γ_t^{-1} . Measuring Γ_t directly from P_i allows us to determine W over a large dynamic range.

Using these methods, we measure W as a function of magnetic field. The data are plotted in Fig. 3(a). At low fields, the relaxation rate becomes very slow: we measure $T_1 = 170$ ms at $B = 1.75$ T. Golovach *et al.* [4] have calculated the relaxation rate caused by spin-orbit coupling between the spin of the electron in the dot and phonons. As inputs to this calculation we use $|g| = 0.38$, which we measure using cotunneling spectroscopy [21], as well as parameters of phonons in GaAs. Also required is $\hbar\omega_0$, the energy level spacing of a parabolic potential well that approximates the confining potential of the dot. We estimate this quantity from the energy of the first excited orbital state and find $\hbar\omega_0 = 2$ meV from transport measurements [16]. The solid line in Fig. 3(a) shows the results of the calculation using these parameters. We find that a spin-orbit length $\lambda_{SO} = 3 \mu\text{m}$ gives a curve that agrees well with our data. The contribution of the Dresselhaus and Rashba terms to λ_{SO} depends on the orientation of the GaAs crystal with respect to the magnetic field. For our orientation [22] and assuming a symmetric parabolic well, we have $\lambda_{SO}^{-1} = |\lambda_\alpha^{-1} - \lambda_\beta^{-1}|$ where $\lambda_\alpha = \hbar/m^*\alpha$, $\lambda_\beta = \hbar/m^*\beta$, and α and β are the Rashba and Dresselhaus spin-orbit terms respectively in the Hamiltonian $H_{SO} = \beta(-p_x\sigma_x + p_y\sigma_y) + \alpha(p_x\sigma_y - p_y\sigma_x)$ [4]. This value of λ_{SO} is in good agreement with measurements

of spin-orbit length scales obtained from antilocalization measurements in quantum dots [23].

We can also extract the value of Γ_e/Γ_t as a function of field. From our fits to data such as those in Fig. 2(f) and (g), we are able to extract $\eta\epsilon_i\Gamma_e/\Gamma_t$ and ϵ_i . We can obtain η by noting that $\eta = (R - W)/R$, where $R = \Gamma_{off} + W$ and is measured directly from histograms such as those in Fig. 2(a) and (b). This allows us to obtain Γ_e/Γ_t at each value of magnetic field. These values are plotted in Fig. 3(b). We see the values are independent of field and very close to 0.5 as we expect.

Using our real-time readout technique, we measure W as a function of B down to very low magnetic fields. We find the relaxation rate increases with field, as predicted by theory [4, 5]. A quantitative comparison between our measurements and theory gives good agreement, demonstrating that spin-orbit coupling can account for spin relaxation in single quantum dots with one electron.

We are grateful to V. N. Golovach and D. Loss for discussions and to V. N. Golovach for providing his Mathematica code to perform the calculations. We are also grateful to I. J. Gelfand and T. Mentzel for experimental help. This work was supported by the US Army Research Office under Contract W911NF-05-1-0062, by the National Science Foundation under Grant No. DMR-0353209, and in part by the NSEC Program of the National Science Foundation under Award Number PHY-0117795.

* Electronic address: samasha@mit.edu

- [1] D. Loss and D. P. DiVincenzo, Phys. Rev. A **57**, 120 (1998).
- [2] J. R. Petta *et al.*, Science **309**, 2180 (2005).
- [3] L. P. Kouwenhoven *et al.*, in *Mesoscopic Electron Transport*, edited by L. L. Sohn, L. P. Kouwenhoven, and G. Schön (Kluwer Academic Publishers, 1997), NATO ASI Series E 345, pp. 105–214.
- [4] V. N. Golovach *et al.*, Phys. Rev. Lett. **93**, 016601 (2004).
- [5] A. V. Khaetskii and Y. V. Nazarov, Phys. Rev. B **64**, 125316 (2001).
- [6] V. I. Fal'ko *et al.*, Phys. Rev. Lett. **95**, 076603 (2005).
- [7] T. Fujisawa *et al.*, Physica B **298**, 573 (2001).
- [8] R. Hanson *et al.*, Phys. Rev. Lett. **91**, 196802 (2003).
- [9] J. M. Elzerman *et al.*, Nature **430**, 431 (2004).
- [10] R. Hanson *et al.*, Phys. Rev. Lett. **94**, 196802 (2005).
- [11] G. Granger *et al.*, Phys. Rev. B **72**, 165309 (2005).
- [12] M. Ciorga *et al.*, Phys. Rev. B **61**, R16315 (2000).
- [13] M. Field *et al.*, Phys. Rev. Lett. **70**, 1311 (1993).
- [14] S. Amasha *et al.*, Proc SPIE **6244**, 624419 (2006).
- [15] S. Amasha *et al.*, (2006), in preparation.
- [16] K. MacLean *et al.*, (2006), in preparation.
- [17] W. Lu *et al.*, Nature **423**, 422 (2003).
- [18] R. Schleser *et al.*, Appl. Phys. Lett. **85**, 2005 (2004).
- [19] L.-X. Zhang *et al.*, Appl. Phys. Lett. **85**, 2628 (2004).
- [20] M. Pioro-Ladrière *et al.*, Phys. Rev. B **72**, 115331 (2005).
- [21] A. Kogan *et al.*, Phys. Rev. Lett. **93**, 166602 (2004).

- [22] The 2DEG is in the [001] plane and the magnetic field is along the axis defined by the $[\bar{1}10]$ and $[1\bar{1}0]$ directions.
- [23] D. M. Zumbühl *et al.*, Phys. Rev. Lett. **89**, 276803 (2002).